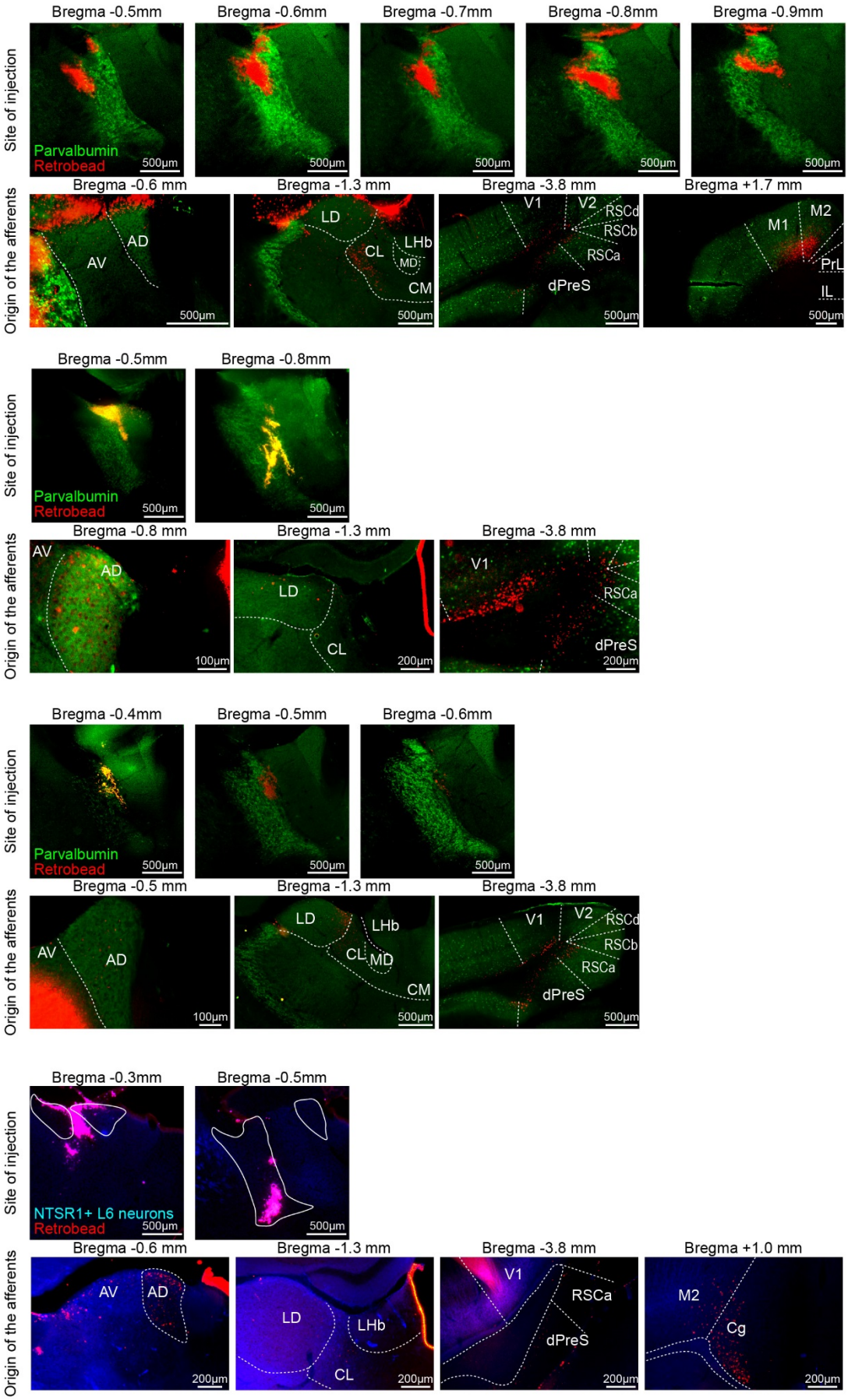
Site of injection
Bregma -0.5mm
Bregma -0.6mm
Bregma -0.7mm
Bregma -0.8mm
Bregma -0.9mm
Parvalbumin
Retrobead
500µm
Origin of the afferents
Bregma -0.6 mm
Bregma -1.3 mm
Bregma -3.8 mm
Bregma +1.7 mm
AD
AV
LD
CL
LHb
MD
CM
V1
V2
RSCd
RSCb
RSCa
dPreS
M1
M2
PrL
IL
Site of injection
Bregma -0.5mm
Bregma -0.8mm
Parvalbumin
Retrobead
500µm
Origin of the afferents
Bregma -0.8 mm
Bregma -1.3 mm
Bregma -3.8 mm
AV
AD
LD
CL
V1
RSCa
dPreS
100µm
200µm
Site of injection
Bregma -0.4mm
Bregma -0.5mm
Bregma -0.6mm
Parvalbumin
Retrobead
500µm
Origin of the afferents
Bregma -0.5 mm
Bregma -1.3 mm
Bregma -3.8 mm
AV
AD
LD
LHb
CL
MD
CM
V1
V2
RSCd
RSCb
RSCa
dPreS
100µm
500µm
Site of injection
Bregma -0.3mm
Bregma -0.5mm
NTSR1+ L6 neurons
Retrobead
500µm
Origin of the afferents
Bregma -0.6 mm
Bregma -1.3 mm
Bregma -3.8 mm
Bregma +1.0 mm
AV
AD
LD
LHb
CL
V1
RSCa
dPreS
M2
Cg
200µm

Supplementary Figure 1. The anterior TRN receives afferents from ATN+, RSC, PreS, cingulate, visual and motor cortices.

(A-D) Five Epifluorescent micrographs of mouse coronal brain sections showing the full extent of a retrobead (red) injection into the anterior portion of the TRN (top) and brain regions where retrobeads were retrogradely transported, thus indicating afferent origin (bottom). **(A-C)** immunostaining for PV (green). **(D)** Immunostaining for NTSR1+ L6 cortical neurons and their projection to the thalamus (blue). Anterodorsal thalamus (AD) – Anteroventral thalamus (AV) – Laterodorsal thalamus (LD) – Mediodorsal thalamus (MD) – Lateral habenula (LHb) – Centrolateral thalamus (CL) – Centromedial thalamus (CM) – Cingulate cortex (Cg) – prelimbic/infralimbic cortex (PreL/IL) – Dorsal presubiculum (dPreS) – Retrosplenial cortex (RSC) – Visual cortex (V1/V2) – Motor cortex (M1/M2) – Prelimbic cortex (PrL) – Infralimbic cortex (IL).

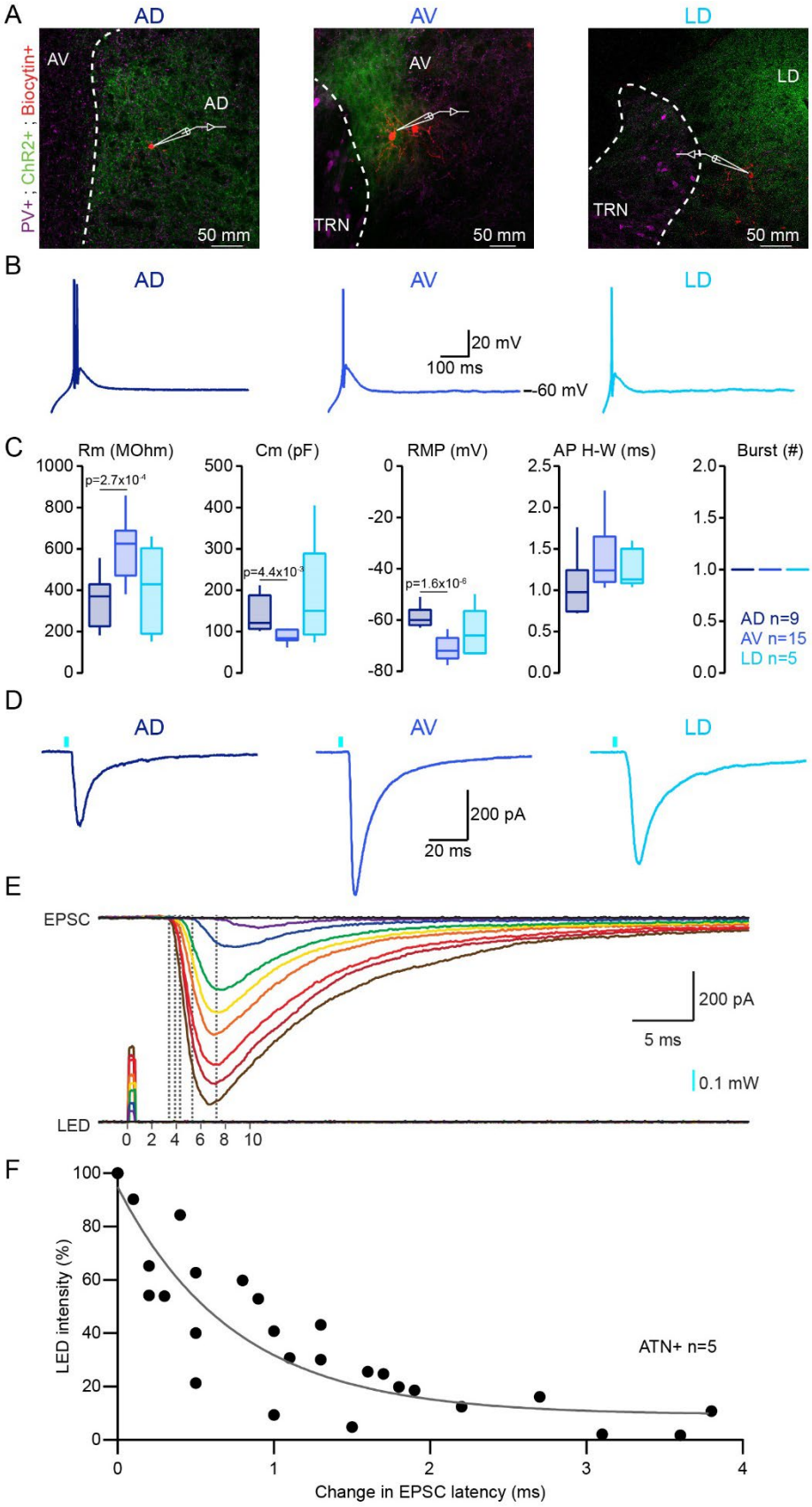
A
AD
AV
LD
PV+ ; ChR2+ ; Biocytin+
AV
AD
50 mm
AV
TRN
50 mm
LD
TRN
50 mm
B
AD
AV
LD
20 mV
100 ms
-60 mV
C
Rm (MOhm)
p=2.7x10-4
Cm (pF)
p=4.4x10-3
RMP (mV)
p=1.6x10-6
AP H-W (ms)
Burst (#)
AD n=9
AV n=15
LD n=5
D
AD
AV
LD
200 pA
20 ms
E
EPSC
200 pA
5 ms
0.1 mW
LED
0 2 4 6 8 10
F
LED intensity (%)
ATN+ n=5
Change in EPSC latency (ms)

Supplementary Figure 2. The PreS/RSC establish functional excitatory synapses onto AD, AV and LD.

(A) Confocal micrographs of 300 µm-thick mouse brain sections showing the whole-cell recorded AD (left), AV (middle) and LD (right) neurons filled with neurobiotin (red). Green, ChR2-EYFP-expressing PreS/RSC afferents, magenta, PV+ TRN cells. **(B)** Voltage responses of neurons shown in A to a negative current injection. (C) Box-and-whisker plots of passive and active cellular properties of PreS/RSC-connected AD (green, n=9), AV (orange, n=15) and LD (blue, n=5) neurons. From left to right: Membrane resistance (Rm), membrane capacitance (Cm), resting membrane potential (RMP), action potential (AP) half-width (H-W), burst number. Student's *t* tests were used to compare Vm, Rm and Cm. A Mann-Whitney U test was used for comparing HW. **(D)** Current responses of AD (left), AV (middle) and LD (right) neurons to optogenetic activation (blue bars, 1 ms, 3.5 mW power, 455 nm) of PreS/RSC afferents, recorded at -60 mV. **(E)** Current responses of a thalamic neuron to optogenetic stimulation of PreS/RSC afferents at different intensities. **(F)** Graph showing the increasing latency of the EPSC latency when reducing light stimulation intensity in 5 ATN+ neurons.

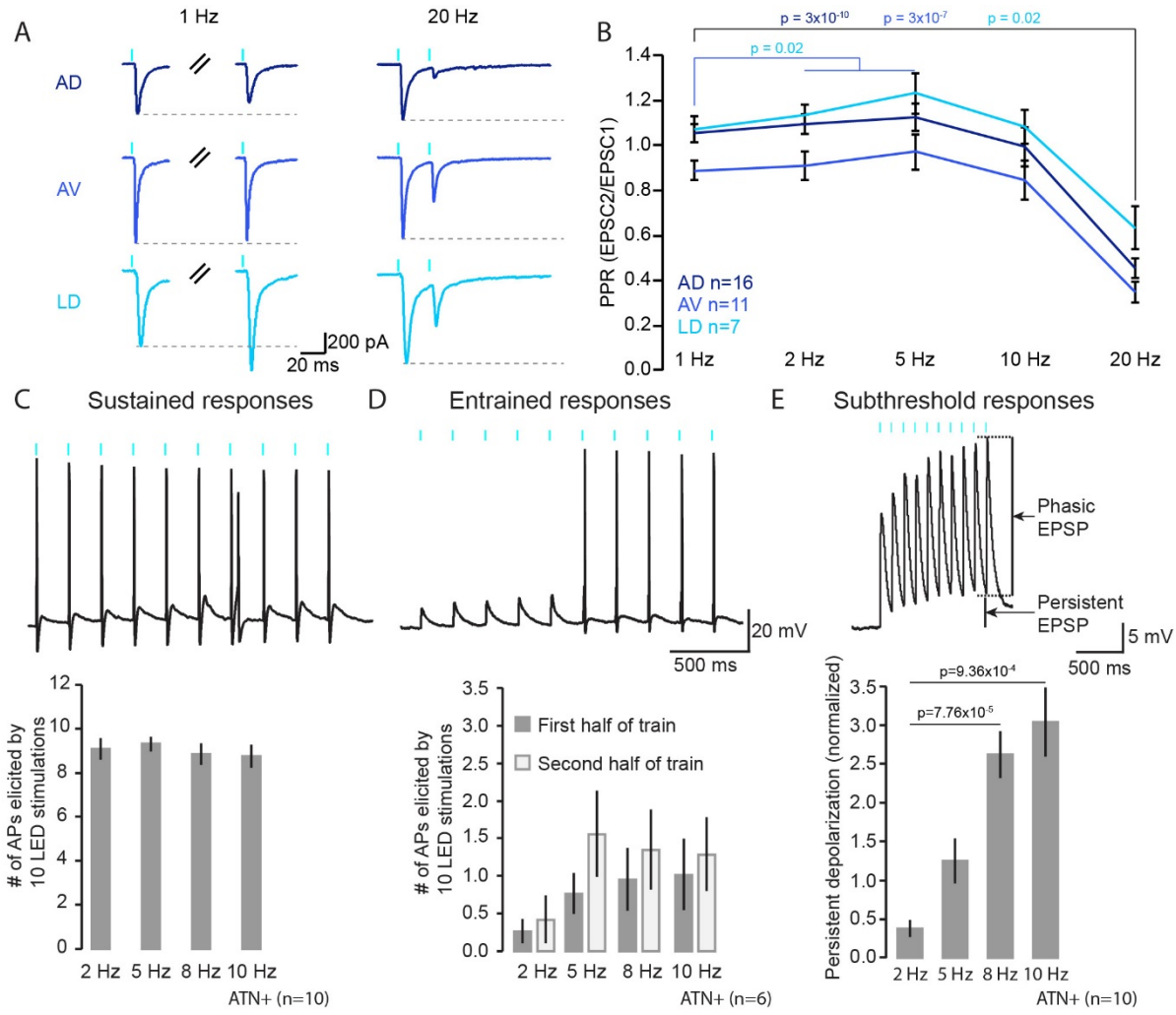

Supplementary Figure 3. The ATN+ receives strong unitary connections with 'driver' characteristics from the PreS/RSC.

(A) Representative current responses of AD, AV and LD neurons held at -60 mV upon paired-pulse stimulation at 1 and 20 Hz. Grey dotted lines correspond to the amplitude of the first EPSC. **(B)** Graph of the paired-pulse ratios. Paired Student's *t* tests with Bonferroni correction for multiple comparisons for PPR at 1 Hz vs PPR at other frequencies ($\alpha = 0.013$). **(C)** Top: typical membrane voltage response of an ATN+ neuron to a train of 10 light stimulations at 10 Hz. Action potentials are elicited from the first light stimulation, classifying it as a sustained response. Bottom: Histogram of action potential numbers during such train stimulations in ATN+ neurons (n = 10) showing sustained response patterns. Wilcoxon signed rank-tests were used to compare between the 2 Hz and the other frequencies of stimulation, with Bonferroni correction for multiple comparison ($\alpha = 0.017$). **(D)** Top: same as in C when neurons responded with a subthreshold response at train onset, classifying them as an entrained response. Bottom: Histogram of action potential numbers during the first half (5 first light stimulation) and the second half of the train of 10 light stimulations in ATN+ neurons (n = 6). A Wilcoxon signed rank-test (at 2 Hz) and Paired Student's *t* tests (at 5, 8, 10 Hz) were used to compare the number of action potentials elicited during the first half vs the second half of the train of stimulation. **(E)** Top: same as in C for subthreshold responses in an ATN+ neuron held at -60 mV. Bottom: Histogram of the persistent depolarization induced by trains in TRN neurons (n = 5). The persistent depolarization was measured on the last 3 stimulations of the train, see methods for the details. Paired Student's *t* tests with Bonferroni correction for multiple comparison ($\alpha = 0.017$) were used to compare the persistent depolarization at 2 Hz with the persistent depolarization at other frequencies.

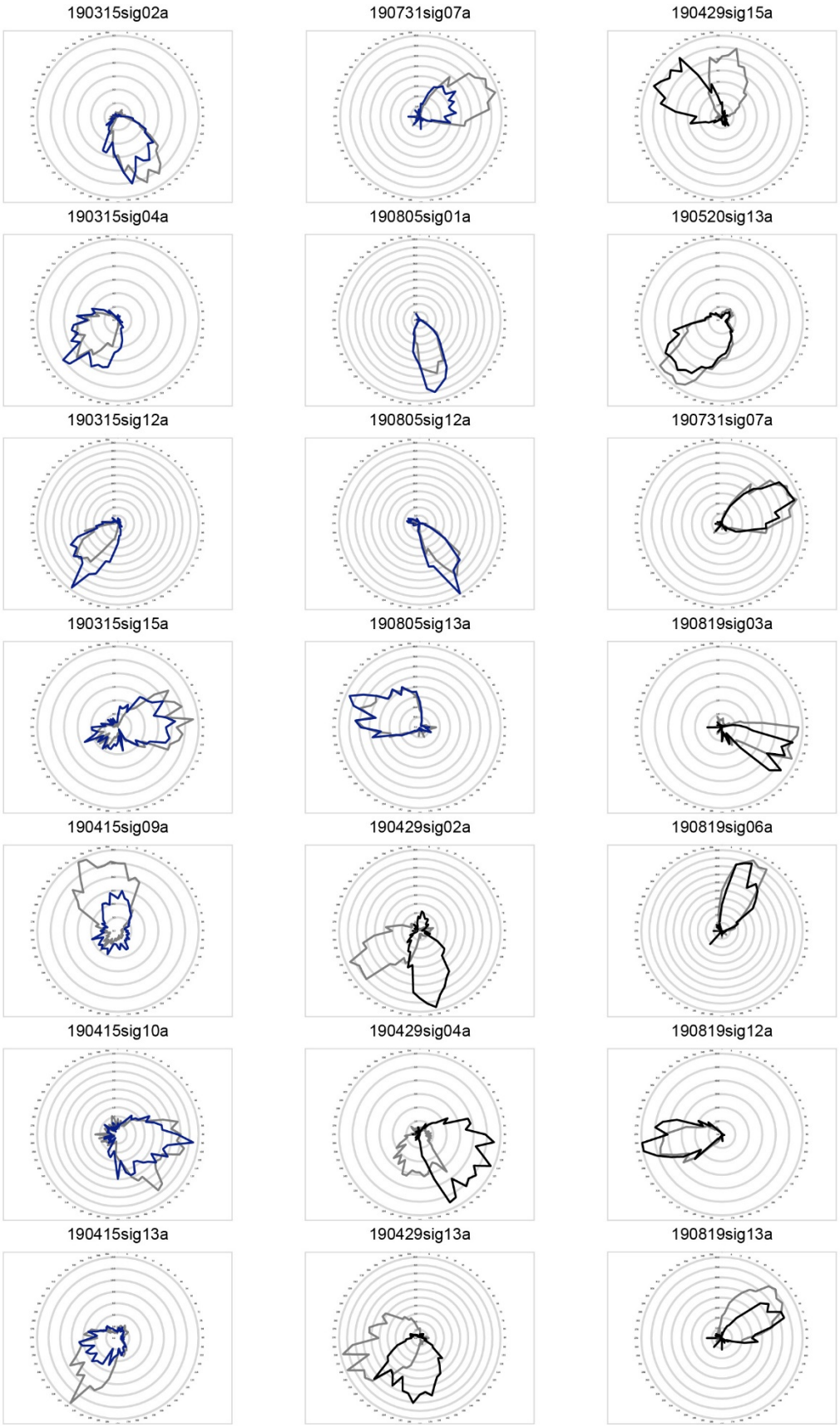

Supplementary Figure 4. Effect of chemogenetic silencing of anterodorsal TRN neurons onto the tuning of thalamic head-direction neurons.

Polar plots of all HD units recorded before (grey) and after CNO (blue) or NaCl (black) injection.

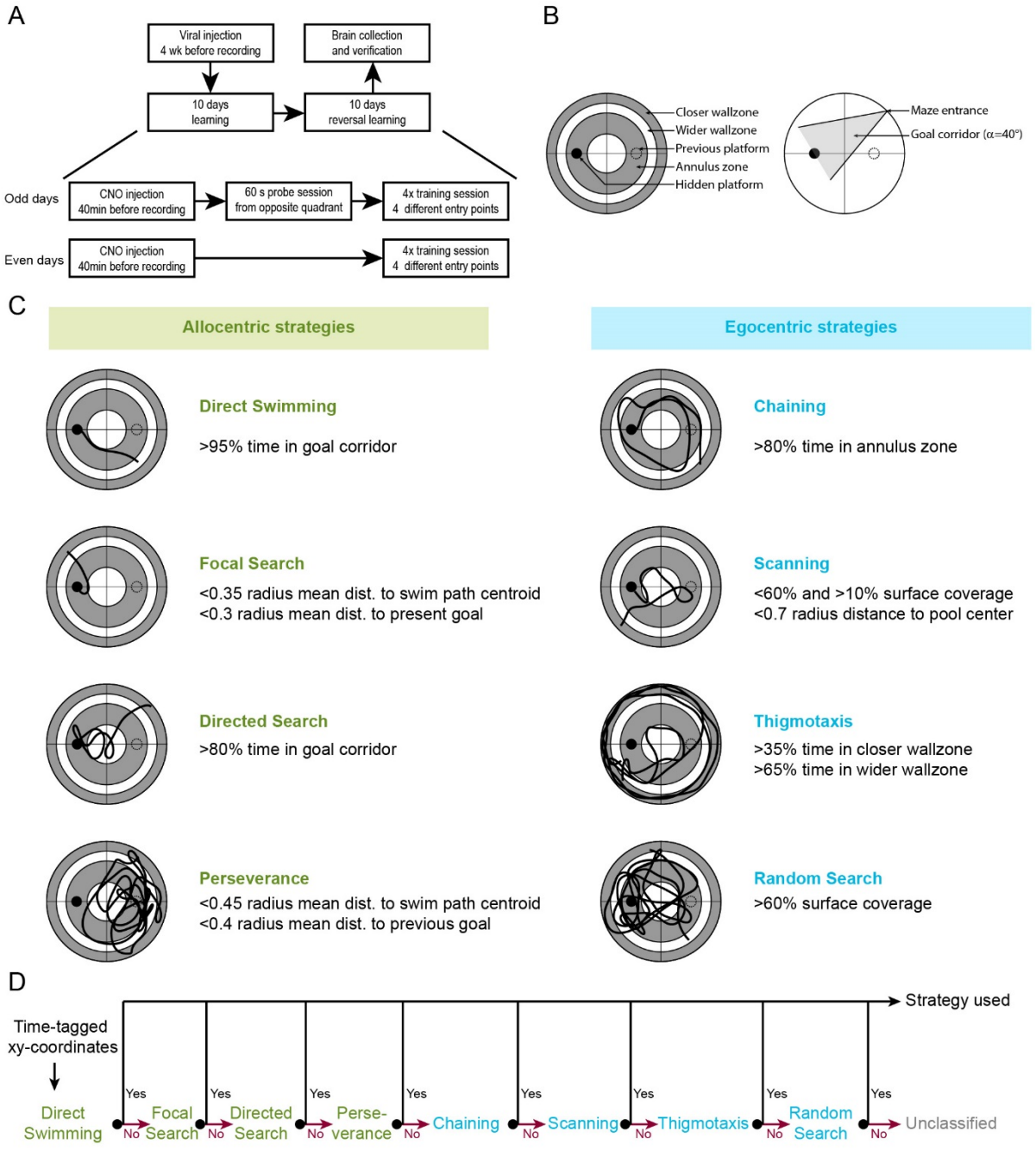

Supplementary Figure 5. Design of Morris Water tasks and algorithm-based classification of search strategies.

(A) Scheme of the experimental design. For further details, see methods. **(B)** Representation of the variables used for the classification process. The pool was divided into several areas to calculate the respective amount of time spent into these specifics areas (left). The average distance of all the data points constituting the search path to its centroid, the present platform and the former platform was used for the classification. Search patterns based on a directional preference for the actual platform were identified using a triangular shaped corridor expanding from the entry point of the mice with its bisecting line towards the platform (right). **(C)** Strategies were identified by one or two parameters representing their major properties. **(D)** The algorithm excluded strategies from the more to the less specific search patterns. Search patterns not recognized were grouped as unclassified strategies.